National Science Center
"Kharkov Institute of Physics and Technology"

Shchagin A.V., Pristupa V.I., Khizhnyak N.A.

ABSOLUTE DIFFERENTIAL YIELD
OF PARAMETRIC X-RAY RADIATION

Preprint

Kharkov - 1993

The results of measurements of absolute differen-
tial yield of parametric X-ray radiation (PXR) in thin
single crystal are presented for the first time. It has
been established that the experimental results are in
good agreement with theoretical calculations according
with kinematical theory. The influence of density ef-
fect on PXR properties is discussed.
7 figs., 19 refs.

* Correspondence to: A.V.Shchagin, Kharkov Ins-
titute of Physics and Technology, 310108 Kharkov,
Ukraine.

Представлены результаты измерений абсолютного диф-
ференциального выхода параметрического рентгеновского
излучения. Сравнение экспериментальных данных с теоре-
тическими показывает справедливость кинематической те-
ории. Обсуждается влияние эффекта плотности на свойст-
ва параметрического рентгеновского излучения.
Рис.7, список лит. – 19 назв.

1 Introduction

Theoretical investigations of radiation generated by the charged particle mov-
ing through a medium with a periodically varying permittivity were per-
formed for the first time in work [1]. Later the radiation in X-ra, band of
charged particle moving through a crystal, has been investigated by Ter-
Mikaelian [2]. Properties of this radiation has been theoretically considered
in works [3 -7,19]. From the middle of 80-ies the experimental investiga-
tions of PXR properties has been provided in the USSR [8 -12]. Later the
investigations in this field has been began in USA [13] and Japan [14].

In our previous paper [10] the investigation of differential PXR character-
istics measured in arbitrary units with high angular and spectral resolutions
at incident electron energy 25 MeV has been carried out. In present work
we have reported the results of measurements of absolute differential yield
of PXR in thin Si single crystal at incident electron energies 15.7 and 25.7
MeV and discuss the influence of density effect on PXR properties at high
incident electron energies.

2 Experimental

The experiment has been made by using the linear electron accelerator LUE-
40 in Kharkov Institute of Physics and Technology. In previous investigation
[10] we have receive the PXR yield in arbitrary units by normalisation of
PXR quanta number on quanta number of characteristic X-ray K-radiation
of target atoms. After setting the experimental procedure of absolute mea-
surements we have carried out the simultaneous investigation of the absolute
K-ionization cross section of the target atoms [18] and PXR absolute yield
[present work].

The experimental setup is shown in fig.1. The beam of accelerated elec-
trons 1 passes in vacuum through a target 2 and a secondary emission monitor
5. The X-ray radiation, induced by electrons in the target, was measured by
a detector 4. The current pulse frequency of the accelerator was 50 Hz, the
pulse duration being 4 μs. The full width at half maximum of the peak in
the spectrum of the accelerated electron beam was 8% of the average electron
energy. The beam spot on the target was nearly 7 mm in diameter, the beam
divergence was about 1 $mrad$. To avoid X-ray spectrum distortions due to

1

the pile up effect the mean beam current value was chosen to be such that the counting rate of the spectrometer should be below 5 Hz. Typically, it was a few nA.

As a target, we used a 17 μm thick silicon single crystal plate, whose crystallographic plane ($\bar{2}20$) was parallel to the plate surface. The target was placed in the vacuum goniometer and was prealigned so that the $< \bar{2}20 >$ axis should be parallel to the velocity vector $\vec{V}$ of the beam electrons, and the crystallographic plane ($\bar{1}11$) should be perpendicular to the detection plane and parallel to the vector $\vec{V}$. The measurements of orientational dependencies in figs.2-5 were provided as a function of target rotation angle ϕ relative axis perpendicular to the detection plane in direction of the detector.

The charge of the beam that has passed through the target during the exposure time was measured by a secondary-emission monitor 5, placed 20 cm behind the target 2, and the charge-to-code converter 7. The monitoring system was calibrated by means of the Faraday cup of the accelerator.

The spectra were measured using the 25 mm^2 area Si(Li) X-ray detector 4 of type BDER-2-25A, with liquid nitrogen cooling. Detector was placed at 4520 mm from the target, at $\theta = 305.9$ mrad to the beam axis, and connected to the goniometer chamber by a vacuum channel. To protect the detector against the electrons scattered in the target, the vacuum channel had a cleaning magnet 3. The detector was surrounded by a lead shield. In front of the 20 μm thick beryllium foil of the detector was placed a lead diaphragm 0.8 mm thick. The angular resolution of the detecting system with taking into account the size of beam spot on the target was about 2 $mrad$. The detector's efficiency was measured with the lead diaphragm through the use of the set of special intensity-calibrated X-ray sources. The energy resolution of the spectrometer at $E_\gamma = 6.4$ keV was found to be 286 eV. Experimental procedure is described in [17]. The absolute measurements technique is described in detail in [18].

3   Results and Discussion

3.1   The PXR peak energies

The X-ray spectra measuring at incident electron energies 15.7 and 25.7 MeV are similar to spectra presented in figs.1,2 in our preliminary work

[10]. Therefore we do not present it in this report text to place economy. In figs.2,3 the peak energies in measured X-ray spectra versus the target orientation are shown by full circles. By solid lines there are shown the calculations of coherent radiation energy according to formula [2, 9,10]·

$$E_{CR} = \hbar\omega_{CR} = \frac{ch\left|\vec{g} \cdot \vec{V}\right|}{c - \sqrt{\epsilon_0}\vec{V} \cdot \vec{\Omega}}, \tag{1}$$

where $\hbar$ is the Planck's constant divided by 2π, ϵ_0 is the constant part of the medium permittivity, $\vec{g}$ is the reciprocal lattice vector, $\vec{\Omega}$ is the unit vector in direction of the detector, c is the light velocity. The solid lines E, D, C, present the calculations by formula (1) for the rows of reciprocal lattice vectors $\vec{g}_{1i}=...< \overline{1}\overline{1}3 >,< 11\overline{1} >...;\ \vec{g}_{2i}=...< \overline{1}\overline{1}5 >, < 111 >, < 33\overline{3} >...;\ \vec{g}_{3i}=...< 004 >,< 220 >...,$ respectively. From this figures one can see that experimental data for all peaks at energies 15.7 and 25.7 MeV are in the same good agreement with calculations of coherent radiation energy according to formula (1). Emphasize, that the radiation connected with reciprocal lattice vector $\vec{g} =< 111 >$ from the row $\vec{g}_{2i}$ is detected with much more intensity comparatively with contribution of other vectors from row $\vec{g}_{2i}$ because the center of reflex from plane (111) at $\phi = \theta/2$ is directed to the detector, whereas all the rest reflexes from vectors of rows $\vec{g}_{1i}, \vec{g}_{2i}, \vec{g}_{3i}$ are directed at large angles to the detector. Peaks in spectra connected with rows $\vec{g}_{1i}$ and $\vec{g}_{3i}$ are caused by the sum of radiations from reciprocal lattice vectors, which compose these rows. From the formula (1) one can see that all vectors of each row have identical radiation energy in our experimental geometry because the line on which vectors come to end is perpendicular to $\vec{V}$. The agreement of experimental data for all observed peaks (see fig.1 in ref. [10])with calculation by formula (1) confirms the coherence of radiation in the vicinity and at large angular distance from centers of PXR reflexes.

Note that in our experiments the registration of the coherent radiation weak peaks at large angular distance from the centers of PXR reflexes was possible due to high spectral and angular resolutions of detecting system, its matching close to optimum one and also low background spectra.

For comparison, the calculations of energies determined by the Bragg law in crystal for detector direction are presented by dashed lines in figs.2,3.

$$E_\theta = \frac{ch\left|\vec{g}\right|^2}{2\sqrt{\epsilon_0}\left|\vec{\Omega}\quad\vec{g}\right|} \tag{2}$$

The calculation according to (2) for the reciprocal lattice vector $\vec{g}$ =< 111 > (line B) is close to experimental data and calculation according to (1) at $\phi \approx \theta/2$ when the PXR reflex center from (111) plane is in the vicinity of the detector direction, but the divergence is increased with disorientation increasing. The calculation according to (2) for the reciprocal lattice vector $\vec{g}$ =< 220 > (line A) has given the lowest energy in comparison with other vectors of the row $\vec{g}_{3i}$, but even this energy much differs from experimental data.

Thus the calculation of energy peaks of PXR according to Bragg formula (2) has given values close to experimental values only in direction close to the PXR reflex center direction. In common case the energies of PXR peaks are described by formula (1) which takes into accounts the coherent nature of PXR. It is interesting to note that the coherent radiation energy of the particle moving in periodical media described by formula (1) does not depend on the concrete interaction mechanism. For example, this formula is true both for coherent bremsstrahlung radiation [2, 15], arising due to the interaction of particle with nuclear crystal subsystem, and for PXR, arising due to the interaction of particle with electron crystal subsystem.

The experimental and theoretical results shown on figs. 2,3 is excellent demonstration of precision smooth tuning possibilities for PXR frequency in a wide X- ray band (see also refs. [9, 10]).

0.3.2   The PXR absolute differential yield

In figs.4,5 the results of measurements of PXR quanta number per electron and unit solid angle are shown by the full circles. The statistical errors of measurements are shown by vertical lines. The absolute measurement error was not exceed ±15%.

The angular resolution of measurements was much less than the angular size of PXR fine structure. The multiple scattering of the incident electrons in the thin target was insignificant. Therefore we have compare our experimental data with calculation of PXR differential yield. The calculations

4

were provided by formula for the number of quanta derived in ref.[10] in accordance with the kinematical theory [2]

$$
\frac{dN}{nd\Omega} = \frac{e^2\omega L \left|\chi_{\vec{g}}(\omega)\right|^2}{2\pi\hbar c_2^3 V\left(\frac{1}{\sqrt{\epsilon}} - \vec{V}\cdot\vec{n}\right)}\cdot
$$

$$
\left|\frac{\left(\omega\sqrt{\epsilon_0}/c\right)\vec{n}\times\left[(\omega\epsilon_0/c^2)\,\vec{V}+\vec{g}\right]}{\left[\left(\omega\sqrt{\epsilon_0}/c\right)\vec{n_\perp}-\vec{g_\perp}\right]^2+\left(\frac{\omega_1^2}{c^2}\right)\left[(mc^2/E_e)^2+\left(\frac{V}{c}\right)^2(1-\epsilon_0)\right]}\right|^2 \qquad (3)
$$

where dN is the number of quanta with frequency $\omega = \omega_{CR}$ (1) emitted in the solid angle $d\Omega$ as n particles with the charge e and energy E_e pass through a crystal of a thickness L; $\chi_{\vec{g}}(\omega)$ is the Fourier component of the variable part of permittivity; $\vec{n_\perp}$, $\vec{g_\perp}$ are the components of $\vec{n}$, $\vec{g}$ perpendicular to $\vec{V}$. Later the similar formula was derived in ref. [7] from semi-quantum expression. The results of calculations of the PXR absolute differential yield for the radiation associated with the reciprocal lattice vector $\vec{g} = < 111 >$ are shown by the lines in figs. 4,5. The contribution from other vectors of the row $\vec{g_X}$ in peak is much less than 1%.

The dashed line is the calculation without taking into account the PXR attenuation in target, the solid line is the calculation with taking it into account. For calculation without attenuation we have use factor $L = \frac{T}{\left|\vec{t}\cdot\vec{v}\right|}$. For the attenuation be taken into account we have use the factor L in the form

$$
L = T_e\cdot\left|\frac{\vec{t}\cdot\vec{n}}{\vec{t}\cdot\vec{v}}\right|\left[1-\exp\left(-\frac{T}{T_e\left|\vec{t}\cdot\vec{n}\right|}\right)\right] \qquad (4)
$$

where $T_e = T_e(\omega)$ is the e-fold attenuation length of radiation with frequency ω; T is the target plate thickness; $\vec{t}$ is the unit vector perpendicular to the target plane; $\vec{v} = \frac{V}{c}$. The formula (4) is applied to the arbitrary target and detector orientation relatively to the beam for Bragg and Laue geometries.

It is necessary to note the fair agreement of the measured absolute differential yield of PXR with that calculated by the formula (3). Calculations by

5

formulae (6) [19] does not show the asymmetry of the PXR yield relatively of reflex center observed in experiment (see figs 4,5).

3.3 The energy dependencies of PXR properties

From comparison of fig.2 and fig.3 one can see that the quantum energy in PXR peaks is practically independent on the incident electron energy in agreement with formula (1) at $V/c \rightarrow 1$. However, figs.4,5 show the strong dependence of angular distribution and PXR yield from it. Let us consider this dependencies.

In fig.6 the calculation by using formula (3) for the angular distance between right and left maxima of PXR yield from figs.4,5 is shown by the line. It is seen from fig.6 that the angular size of PXR reflex $\Delta\phi$ is decreased with growth of incident electron energy $\Delta\phi \sim mc^2/E_e$ up to the critical energy $E_{crit} = \frac{\hbar\omega_R}{\hbar\omega_p} mc^2$, where $\hbar\omega_R$ is the energy of PXR quanta in the vicinity of the reflex center, ω_p is the plasma frequency for the Si single crystal. In our case $\hbar\omega_R \approx 12.9$ keV and $E_{crit} = 212$ MeV. At $E_e \gg E_{crit}$ the angular size of reflex does not depend on incident electron energies. In fig.6 the experimental results are shown by full circles. It is seen that the experimental results on the angular size of PXR reflex in the region of electron energy $E_e \ll E_{crit}$ are in good agreement with the calculation using formula (3).

In fig.7 the calculations using formula (3) of PXR differential yield in left (solid line) and right (dashed line) maxima of orientational dependencies of PXR yield (see fig.4,5) are shown. It is seen from fig.7 that the PXR differential yield in maxima increases with incident electron energy increasing approximately proportional to the square of energy up to the critical energy E_{crit}. At $E_e \gg E_{crit}$ the PXR differential yield does not depend on the incident electron energy. In fig.7 the results of our measurements are shown by full circles for the left maximum in figs.4,5 and open circles for right ones. One can see that our experimental results on the PXR differential yield in maxima in the region of the incident electron energy $E_e \ll E_{crit}$ are in good agreement with the calculation using formula (3).

Thus, the experimental investigations, (in ref.[10] and in this work), of spectral and angular differential characteristics of PXR, excited in the thin Si crystal in the Laue geometry by relativistic electrons with the energy considerably less than the critical energy confirm fully the validity of the Ter-Mikaelian kinematical theory [2].

4 The influence of density effect on dependence of properties of PXR on incident electron energy

In this section we have consider the physical reason by which the linear decreasing of angular size of PXR reflex (fig.6) and square growth of the PXR differential yield in maxima (fig.7) are stopped with the increase of the incident electron energy at $E_e \approx E_{crit} = \frac{\omega_R}{\omega_p} mc^2$. Also we have consider the influence of density effect on a possibilities of dynamic effect experimental observation.

It is known, that PXR is the result of charged particle virtual photon reflection from the crystallographic plane system of crystal through which the particle moves. By other words the particle field is a radiation source, and the crystallographic plane system is a reflector. It is evidently that the crystal reflecting properties do not depend on the incident electron energy. Therefore the behavior of field of a particle moving through a crystal has the basic influence on energy dependencies of PXR properties. In particular, the field components of incident particle with frequency about ω_R take part in formation of PXR reflex with quantum energy in the reflex center $E_R = \hbar\omega_R$. Let us consider the spectral-angular distribution of virtual photons of relativistic charged particle moving through a media with the average dielectric permittivity ε_0 for photon energy $\hbar\omega \ll E_e$. For this we can use the expression from [16] without the constant factor

$$\frac{dN}{d\omega d\Omega} \sim \omega\varepsilon_0 \left| \frac{\overrightarrow{n} \times \overrightarrow{V}}{\omega - \overrightarrow{k} \cdot \overrightarrow{V}} \right|^2 \tag{5}$$

where $\overrightarrow{k}$ is photon wave vector, $\overrightarrow{n} = \frac{\overrightarrow{k}}{|\overrightarrow{k}|}$. By using the approach $\gamma = 1/\sqrt{1-(v/c)^2} \gg 1$ and $\theta_1 \ll 1$ and also the expression for the dielectric permittivity $\varepsilon_0 = 1-(\omega_p/\omega)^2$ for frequencies exceeding the atomic frequencies one can easy to transform expression (5) to

$$\frac{dN}{d\omega d\Omega} \sim \frac{\varepsilon_0}{\omega} \left[\frac{\theta_1}{\theta_1^2 + 1/\gamma^2 + (\omega_p/\omega)^2} \right]^2 \tag{6}$$

7

where θ_1 is the angle between the particle velocity vector $\overrightarrow{V}$ and photon wave vector $\overrightarrow{k}$, ω_p is the plasma frequency of media electrons. Analysing the expression (6) one can easy to see that angular and energy dependencies of PXR reflex are similar to angular and energy dependencies of distribution of incident particle virtual photons with frequency $\omega = \omega_R$.

In energy region $E_e \ll E_{crit}$, that corresponds to $1/\gamma^2 \gg (\omega_p/\omega_R)^2$, the presence of media have no influence on the distribution (6): maxima in angular distribution are placed at angles $\theta_{1\,max} = 1/\gamma$, and number of quanta in maxima increases as $\frac{dN}{d\Omega} \sim \gamma^2$. This corresponds to the calculations of PXR properties by the formula (3) and is confirmed by our experimental results (fig.6,7). The influence of media in this case is small and distribution of virtual photons (6) is similar to that for a particle moving through a vacuum.

However, at $E_e \gg E_{crit}$, that corresponds to $1/\gamma^2 \ll (\omega_p/\omega_R)^2$, as seen from formula (6), the influence of the media on the particle field leads to independence of the component distribution (6) with a frequency ω_R on the energy of incident electron. In particular $\theta_{1\,max} \to \frac{\omega_p}{\omega_R}$ (in our experimental conditions $\frac{\omega_p}{\omega_R} = 2.4$ mrad). For PXR it means the transition from linear decreasing of reflex angular size to saturation at $E_e \gg E_{crit}$ (as it is seen in fig.6 $\Delta\phi \to 2.4$ mrad at $E_e \gg E_{crit}$), and the transition from square growth of quantum number in maxima to the saturation at $E_e \gg E_{crit}$ (see fig.7). This can be seen from formula (3) after substitution the expression in denominator $\left(\frac{mc^2}{E}\right)^2 + \left(\frac{V}{c}\right)^2 (1 - \epsilon_0)$ to $\frac{1}{\gamma^2} + \left(\frac{V}{c}\right)^2 \left(\frac{\omega_p}{\omega}\right)^2$. Thus the saturation at $E_e \gg E_{crit}$ of the number of quanta, angular size and another properties of PXR reflex take place due to the influence of the density effect of media on the field of incident particle moving through this media. The saturation of some PXR properties was confirmed at $E_e \gg E_{crit}$ experimentally in refs. [11] and [14].

As it is seen from above mentioned consideration we have explain the change of PXR properties behavior on the energy of incident electrons at $E_e \approx E_{crit}$ as influence of density effect on the incident particle field. Note that Ter-Mikaelian in [2] have not discuss the influence of density effect on radiation properties in the vicinity of the Bragg conditions (he names this radiation as "resonance radiation"), although this influence is contained in formulae of his theory [2], and therefore in formula (3).

Unfortunately, the influence of the density effect leads to cessation of the

8

rapid increase of PXR differential yield with increasing energy of incident particles at $E_e \approx E_{crit}$. From above mentioned consideration it is seen that to receive the PXR maximum yield at definite value of ω_R and all other things being equal it is necessary to use crystals with lowest average density of electrons because in this case the density effect influence begin at higher energy of incident electrons.

Let us consider the influence of the density effect on a possibilities of dynamic effect experimental observation. In work [7] the condition in which it is possible to neglect the dynamic effect was derived (if experimental angular resolution mach poorer than $|\chi_{\mathcal{T}}|$) as

$$\frac{1}{\gamma} > |\chi_{\mathcal{T}}| \tag{7}$$

where $\frac{1}{\gamma}$ associated with a width of PXR angular distribution. In condition (7) the influence of the density effect does not taking into account. With taking into account the density effect a width of PXR angular distribution is

$$\sqrt{\frac{1}{\gamma^2} + \left(\frac{\omega_p}{\omega_R}\right)^2} \tag{8}$$

and therefore the condition in which it is possible to neglect the dynamic effect have another form

$$\sqrt{\frac{1}{\gamma^2} + \left(\frac{\omega_p}{\omega_R}\right)^2} > |\chi_{\mathcal{T}}|. \tag{9}$$

The condition (9) put more hard limitation then (7) on a possibilities of dynamic effect experimental observation at high incident electron energy because at $E_e \rightarrow \infty$ relation (9) reduce to form $\sqrt{|\chi_0|} = \frac{\omega_p}{\omega_R} > |\chi_{\mathcal{T}}|$ that usually is satisfy.

Thus density effect taking into account lead to impossibility of dynamic effect for noticeable part of PXR reflex in single crystal even at high incident electron energy.

5   Acknowledgments

Bibliography

[1] Ya.B. Fainberg and N.A. Khizhnyak, Zh. Ehksp. Teor. Fiz. 32 (1957) 883.

[2] M.L. Ter-Mikaelian, High-energy electromagnetic processes in condensed media, Interscience tracts on Physics and Astronomy (Wiley-Interscience, New York, 1972).

[3] V.G. Baryshevskij, Channeling, radiation and reactions in crystals at high energies (BGU prol.; Minsk, 1982) [in Russian].

[4] G.M. Garibyan and C. Yang, X-ray transition radiation (Arm. SSR publ., Erevan, 1983) [in Russian].

[5] D. Dialetis, Phys. Rev. A 17 (1978) 1113.

[6] V.P. Lapko, N.N. Nasonov, Zhurn. Tekhn. Fiz. 60(1990)160.

[7] H. Nitta, Phys. Lett. A 158 (1991) 270.

[8] D.I. Adeishvili, S.V. Blazhevich, V.F. Boldyshev, G.L. Bochek, V.I. Vit'ko, V.L. Morokhovskij and B.I. Shramenko, Dokl. Akad. Nauk SSSR 298 (1988) 844.

[9] V.L. Morokhovskij, A.V. Shchagin, Zhurn. Tekhn. Fiz. 60(1990)147.

[10] A.V. Shchagin, V.I. Pristupa, N.A. Khizhnyak, Phys. Lett. A 148(1990)485.

[11] Yu.N. Adishchev, A.N. Didenko, V.V. Mun, G.A. Pleshkov, A.P. Potylitsin, V.K. Tomchakov, S.R.Uglov, and S.A. Vorob'ev, Nucl. Instrum. Methods Phys. Research B 21 (1987) 49.

[12] R.O. Avakyan, A.Eh. Avetisyan, Yu.N. Adishchev, G.M. Garibyan. S.S. Danagulyan, O.S. Kizogyan, A.P. Potylitsin, S.P. Taroyan, G.M Ehlbakyan, C.Yang, Pis'ma Zh. Ehksp. Teor Fiz. 45 (1987) 313

[13] R.B. Fiorito, D.W. Rule, X.K. Maruyama, K.L. DiNova, S.J. Evertson, M.J. Osborne, D. Snyder, H. Rietdyk, M.A. Piestrup, and A.H. Ho, Phys. Rew.Lett. 71(1993)704.

[14] S. Asano, I. Endo, M. Harada, S. Ishii, T. Kobayashi, T. Nagata, M. Muto, K. Yoshida, H. Nitta, Phys. Rev. Lett. 70 (1993) 3247.

[15] H. Uberall, Phys. Rev. 103 (1956) 1055.

[16] V.A. Bazylev, N.K. Zhevago, Radiation of fast particles in matter and external fields ("Nauka", Moscow, 1987) [in Russian].

[17] D.I. Adeishvili, S.V. Blashevich, G.L. Bochek, V.I. Kulibaba, V.P. Lapko, V.L. Morokhovskij, G.L. Fursov, and A.V. Shchagin, Prib. Tekhn. Ehksp. 3(1989)50; for correction see Prib. Tekhn. Ehksp. 6(1989)4.

[18] A.V. Shchagin, V.I. Pristupa, N.A. Khizhnyak, Nucl. Instr. Meth. Phys. Res. B (to be published).

[19] I.D. Feranchuk and A.V. Ivashin, J. Physique 46(1985)1981.
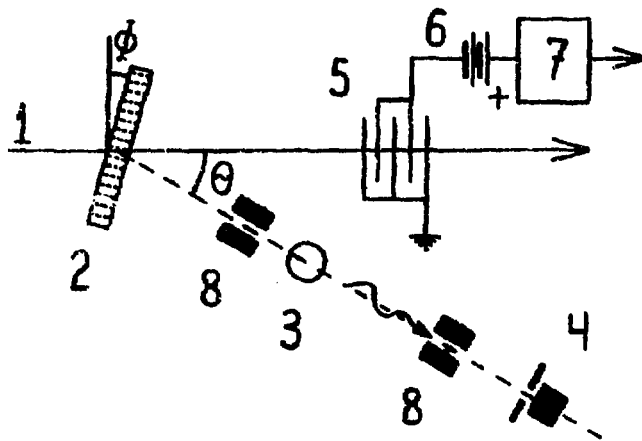
Fig.1. Experimental layout. 1 - electron beam; 2 - Si target; 3 - cleaning magnet; 4 - Si(Li) detector with a diaphragm; 5 - secondary emission monitor; 6 - 100 V battery; 7 - charge- to-code converter; 8 - graphite collimators.
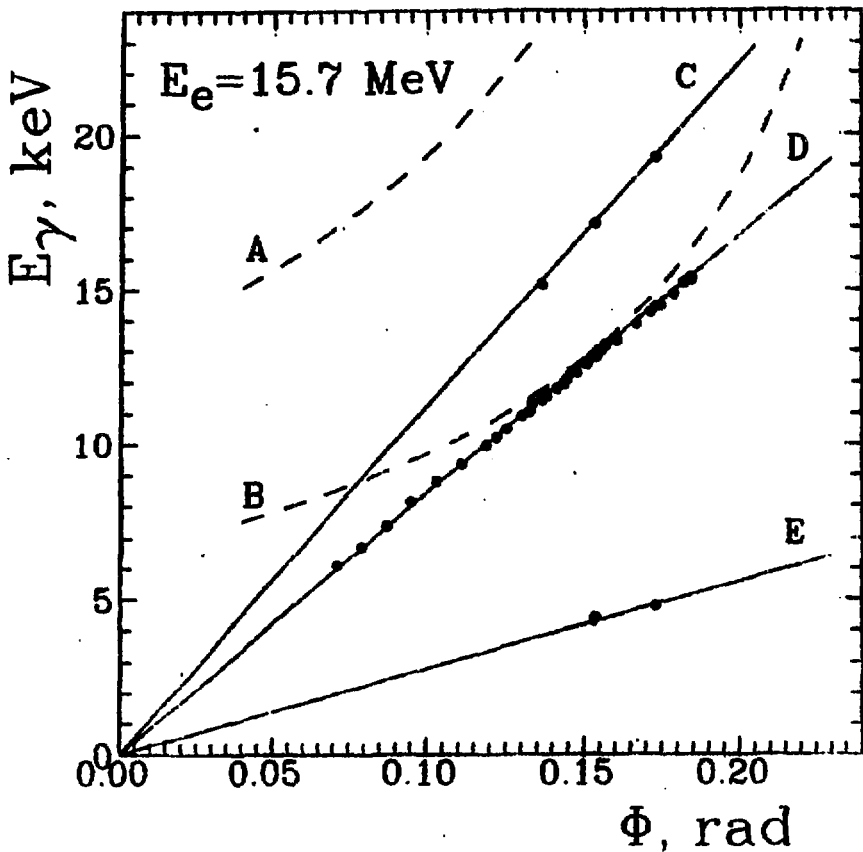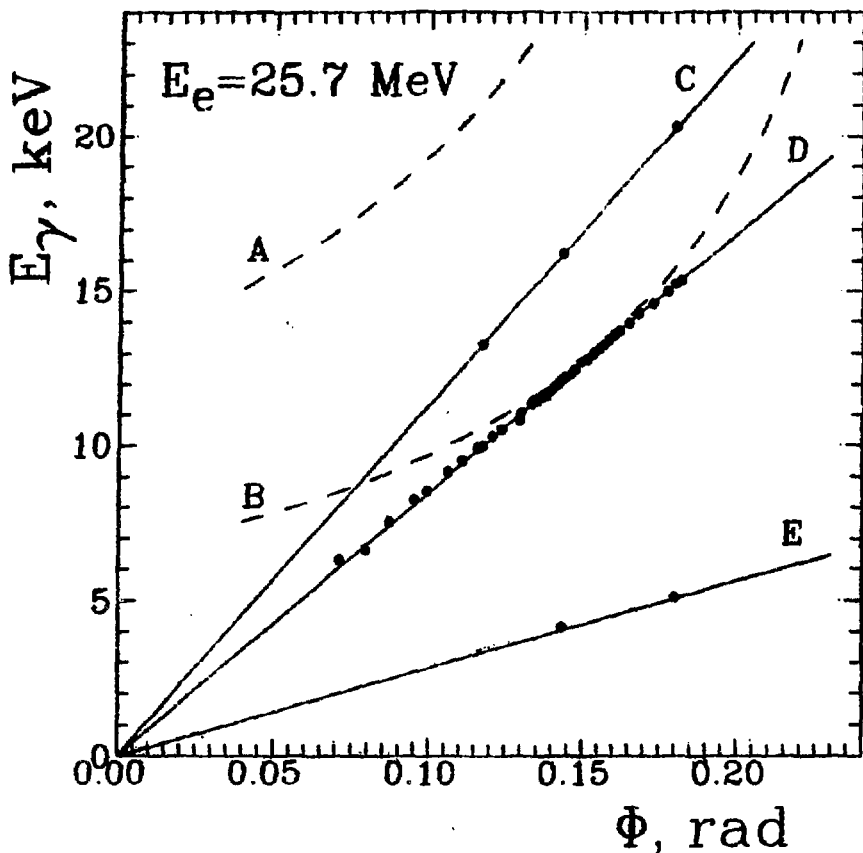
Fig. 2. Peak energies in radiation spectra measured versus the crystal alignment (full circles) at $E_e = 15.7$ MeV. The solid lines E, D, C show the coherent radiation energies calculated by formula (1) for the rows of reciprocal lattice vectors $\vec{g}_{1i}$, $\vec{g}_{2i}$ and $\vec{g}_{3i}$ respectively. The dashed lines B,A is the Bragg energy calculated by formula (2) in the direction of detection for $\vec{g} = <111>$ and $\vec{g} = <220>$ respectively.

Fig. 3. Peak energies in radiation spectra measured versus the crystal alignment (full circles) measured at $E_e = 25.7$ MeV. The solid lines E, D, C show the coherent radiation energies calculated by formula (1) for the rows of reciprocal lattice vectors $\vec{g}_{1i}$, $\vec{g}_{2i}$ and $\vec{g}_{3i}$ respectively. The dashed lines B, A is the Bragg energy calculated by formula (2) in the direction of detection for $\vec{g} = <111>$ and $\vec{g} = <220>$ respectively.
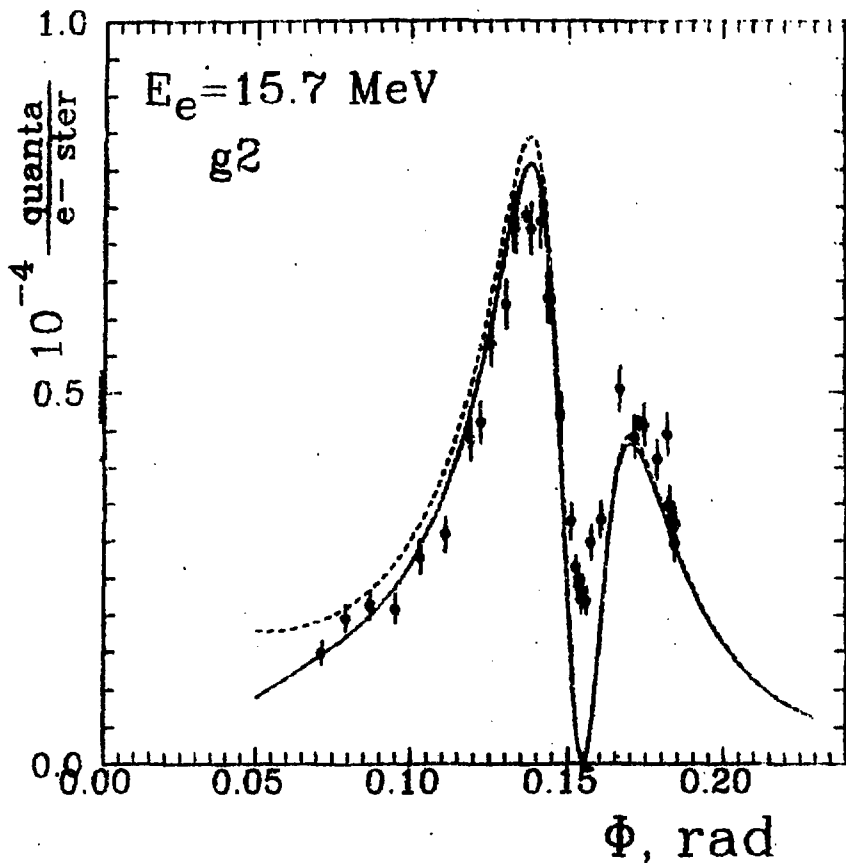
Fig. 4. The number of PXR quanta measured at $E_e = 15.7$ MeV versus the crystal alignment (full circles with statistical errors). The dashed line is the calculation by formula (3) for $\vec{g} = <111>$ without attenuation taking account, the solid line shows the calculation taking into account the PXR attenuation in the target.
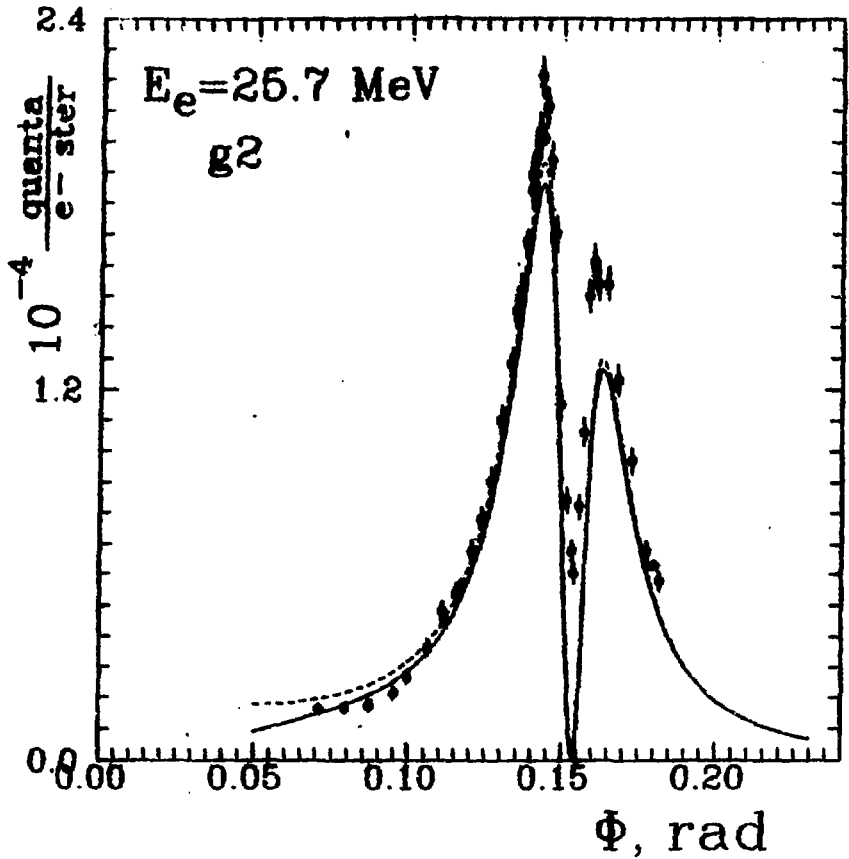
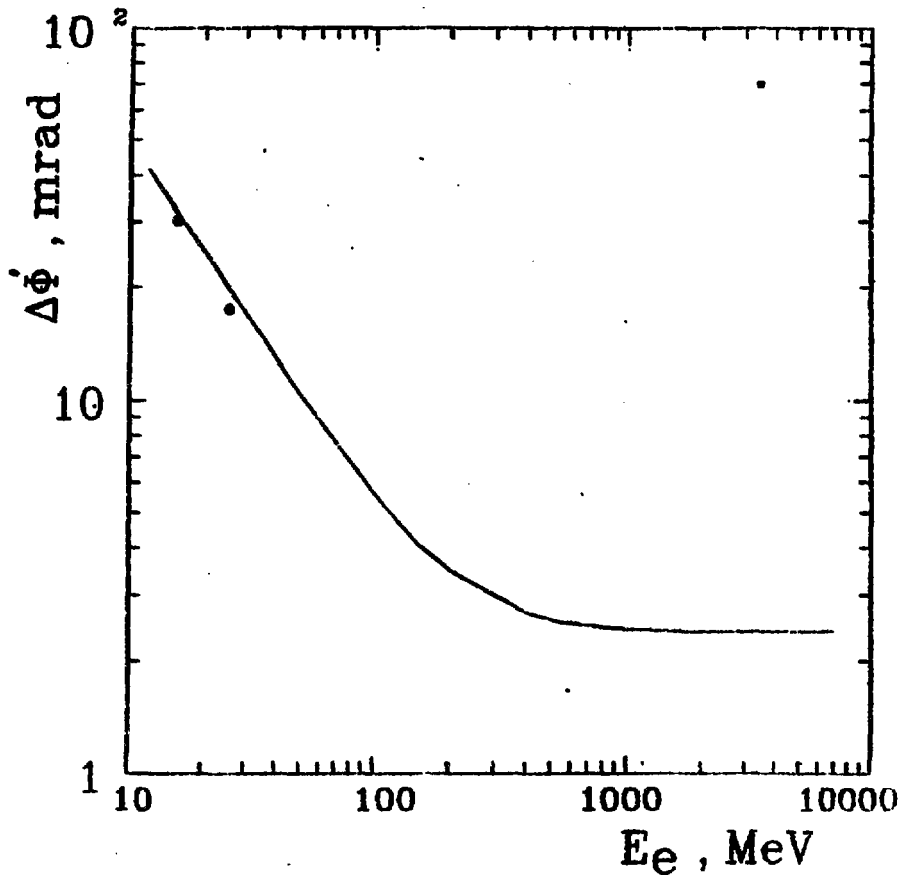Fig. 5. The number of PXR quanta measured at $E_e = 25.7$ MeV versus the crystal alignment (full circles with statistical errors). The dashed line is the calculation by formula (3) for $\vec{\tau}^* = <111>$ without attenuation taking account, the solid line shows the calculation taking into account the PXR attenuation in the target.

Fig. 6. The angular distance between left and right maxima in fig.4,5 versus the incident electron energy. Full circles are experimental data, line is calculation using the formula (3).
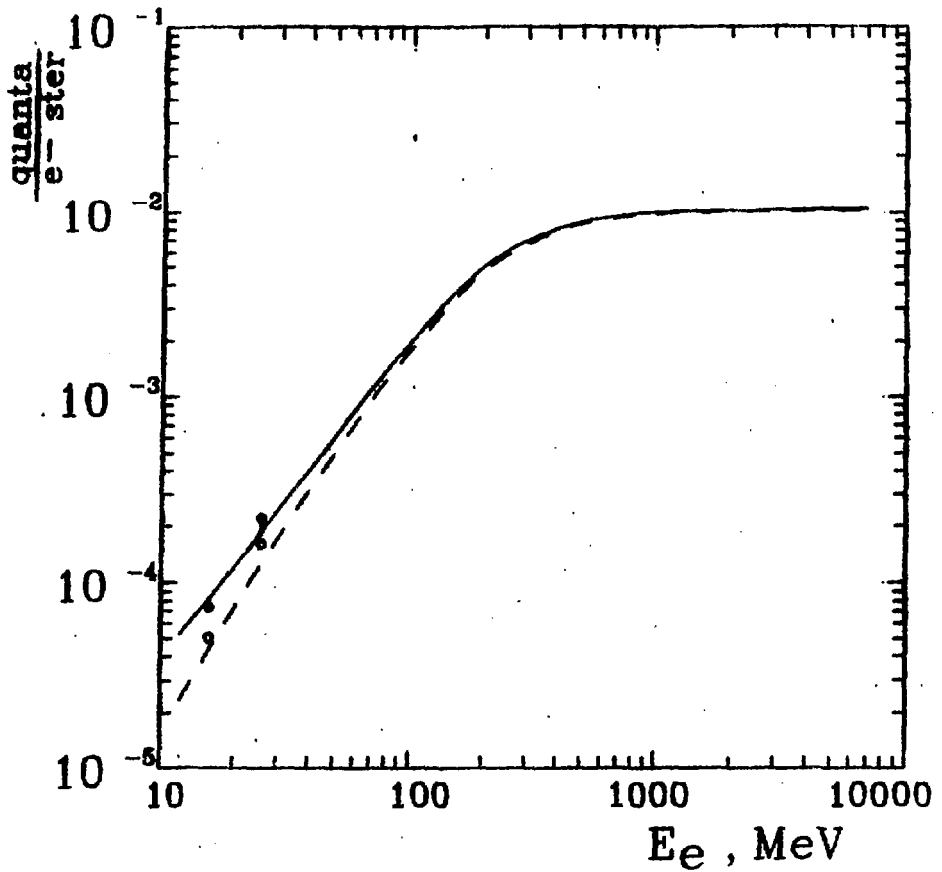
Fig. 7. The differential yield of PXR quanta in left (full circles and solid line) and right (open circles and dashed line) maxima from figs.4,5 versus the incident electron energy. The calculation using formula (3) shown by lines, circles are experimental data.